J Electroceram (2017) 38:24–42
DOI 10.1007/s10832-016-0054-x

FEATURE ARTICLE

Electric field assisted sintering of electroceramics and in situ analysis by impedance spectroscopy

R. Muccillo[1] · **E.N.S. Muccillo**[1]

Received: 25 April 2016 / Accepted: 20 October 2016 / Published online: 30 October 2016

Abstract Since the first report several years ago on pressureless sintering of yttria-stabilized zirconia with several seconds at relatively low temperatures by application of an electric field, an increasing number of scientific reports have been published on sintering ion conducting, semiconducting and insulating polycrystalline electroceramics. The electric field-assisted sintering consists in applying an electric field either during heating up or under isothermal conditions at temperatures well below the ones applied during conventional sintering. Besides the lower temperatures, shorter times are required to achieve full densification without considerable grain growth, evidencing the potential of this technique for obtaining functional electroceramics with improved mechanical and electrical properties at lower costs. Even though some mechanisms have been suggested, the description of the phenomenon at the microscopic level leading to full densification with seconds remains a challenge. We report in situ electrochemical impedance spectroscopy of an ionic conductor (ZrO_2: 8 mol% Y_2O_3), a proton conductor ($BaCe_{0.8}Zr_{0.1}Y_{0.1}O_{3-\delta}$) and a semiconductor ($SnO_2$: 0.5 mol% MnO_2) performed during conventional and electric field-assisted sintering experiments. Attention is also directed on the description of the experimental setups and procedures and to the evaluation of microstructural details by scanning electron microscopy. The analysis of the in situ impedance spectroscopy diagrams under heating (before either conventional or electric field-assisted sintering) and under cooling (after) provides evidence of densification with pore elimination and welding of grains. Prospects for future experimental and simulation research work are outlined.

Keywords Electric field assisted sintering · In situ impedance spectroscopy · Dilatometry · Electroceramics

1 Introduction

1.1 Electric field-assisted (flash) sintering

Sintering is the most important step towards the consolidation of either porous or dense ceramic components. It is a thermally activated process that produces continuous modifications in the compact microstructure and usually takes hours to reach full density. The conventional sintering of ceramic materials consists in heating a ceramic powder compact under an established profile (heating rate, dwelling temperature and time, cooling rate, and atmosphere) that depends, in part, on their phase diagram [1, 2].

There are many ways to provide additional energy to enhance sintering, and thereby accelerating its kinetics, i.e., lowering temperature and time to achieve a desired density: 1- by applying pressure during heating (hot-pressing and hot isostatic pressing); 2- using sintering aids with melting point lower than that of the ceramic being sintered (liquid phase sintering); 3- using unconventional heating sources such as microwave heating and high power laser beams; and 4- applying electric fields with or without pressure (electric field-assisted sintering).

The discovery that alumina doped with MgO could sinter to theoretical density demonstrated that sintering could produce superior microstructures by the proper combination of

✉ R. Muccillo
muccillo@usp.br

E.N.S. Muccillo
enavarro@usp.br

[1] Center of Science and Technology of Materials, Energy and Nuclear Research Institute, S. Paulo, Brazil

sintering variables - time, temperature, dopant, particle size distribution, as reported on 1990 [3]. Another sintering variable was added later: the electric field, which can produce an electric current flow *either* through a graphite die containing the specimen under mechanical load, *or* through the ceramic compact powder itself, without pressure, as will be described below. These techniques, looking for enhancement of the sintering process, have been reported in several review papers [4–7].

Electric field-assisted sintering is usually performed according to two main experimental procedures:

- Low electric field (of the order of volts) and high electric currents (kAmps) through a *graphite die* containing the specimen under load; originally it was named spark plasma sintering [7]. There is no agreement whether the plasma phenomenon happens in these experiments.
- High electric field (tens or hundreds of volts) and low electric currents (up to Amps) through *the specimen* without pressure; originally it was named flash sintering [8]. This is one of the focuses of this Feature Article.

In 2009 it was shown that heating under a DC electric field as small as 4 V/cm could densify a ZrO_2: 3 mol% Y_2O_3 (3YSZ) ceramic compact with reduced grain growth in comparison with heating without the electric field [8]. Subsequently, the technique was applied to 3YSZ with 20 V/cm DC electric field under heating from room temperature, producing dense ceramics with reduced average grain size, at temperatures below the conventional ones [9]. After these pioneering papers, a large number of papers were published on the application of electric fields to many electroceramics with different electrical behavior: ion conductors, mainly stabilized zirconia [8–32] and ceria [33–35], semiconductors [36–50], insulators [51–54], proton conductors [55, 56], and others [57–65] (see Table 1). "Fast sintering" and "flash sintering" are the terms used when densification is accelerated (relative to zero field - conventional sintering) and when it happens in few seconds, respectively. For the majority of the studied electroceramics, the transition from "fast" to "flash" is observed for DC electric fields of magnitude ~150 V/cm. This transition, however, depends on the electrical behavior of the electroceramic and whether the electric field is applied during the whole heating procedure, or isothermally, or under specific experimental procedures. A combination of flash sintering and spark plasma sintering has also been proposed for sintering SiC, B_4C and ZrO_2: 3 mol% Y_2O_3 (3YSZ) [66–69].

Several possible reasons for the flash sintering phenomenon were suggested: modification of the space charge defect chemistry at the grain boundaries, production of additional driving force for grain growth, alteration of the interface energy, creation and migration of Frenkel pairs, and Joule heating at the grain boundaries [9, 10, 16, 18, 70–76].

The experimental details, the results and the discussions in the references listed in Table 1 provide information on the effects of many intrinsic (average particle size, packing density, sample size and shape) and extrinsic parameters (electric field strength, limit of electric current density, electric power, temperature profile, etc.). Even though several intrinsic and extrinsic factors related to flash sintering have been explored, the description of the mechanism(s) behind the actual sintering process remains a challenge. Joule heating is obviously the primary consequence of electric current pulses delivered through the electroceramic. The majority of the papers in Table 1 deal with the effect of the electric field on densification and microstructure, with emphasis on the possibility of densification at temperatures lower than previously reported, besides achieving lower average grain size. The reports on mechanical properties (fine microstructure should produce specimens with improved mechanical properties) are scarce and some take into consideration the electrical properties (flash sintering is an electrical phenomenon!) [12, 20, 21, 24, 25, 28, 45, 56, 59, 61, 65, 67]. All experiments reported by the following authors describe in situ impedance spectroscopy results [12, 21, 25, 55] while all the others describe ex situ data [20, 24, 28, 45, 59, 61, 65].

1.2 Impedance spectroscopy

The impedance spectroscopy technique consists in applying a low amplitude AC electric signal, measuring the corresponding electrical current with their ratio determining the impedance

Table 1 Flash-sintered electroceramics

Electrical behavior	Maaterial
Ion conductor	YSZ [8–32, 66], GDC [33–35], β-Alumina [65]
proton Conductor	BCGd [55], BZCYYb [56]
Semiconductor	Co_2MnO_4 [36, 44], $SrTiO_3$ [37], SnO_2 [38], SnO_2:Mn [39], SiC [40, 67, 68], $BaTiO_3$ [45, 46], ZnO [43, 48–50], TiO_2 [41, 42], $KNbO_3$ [47], B_4C [69]
Insulator	Al_2O_3 [51], Y_2O_3 [52], Ca-Phosphate [53], ZrB_2 [54]
Other	Al_2O_3-YSZ [57, 59], Al_2O_3-TiO_2 [60], LSCF-CeO_2 [58, 61], Al_2O_3-$Y_3Al_5O_{12}$-ZrO_2 [62], SOFC [63], LSCF [64]

$[Z(\omega) = Re\ Z - i\ Im\ Z] \equiv [Z' - i\ Z'']$, with $\omega = 2\pi f$ [77], f being the frequency of the AC signal. Figure 1 shows a typical $[-Z''(\omega)\ x\ Z'(\omega)]$ impedance diagram of an yttria-stabilized zirconia (ZrO_2: 8 mol% Y_2O_3) polycrystalline ceramic, composed of high (HF) and low (LF) frequency semicircles due, respectively, to the bulk (grains) and interfaces (mainly grain boundaries) contributions to the electrical resistivity. The electrode polarization, which occurs at even lower frequencies [78], is not shown. The resistance R is determined at the intersection of the semicircle with the real (x) axis; the depression angle β is an indication on how homogeneous is the distribution of the components responsible for the semicircles (HF - grain size distribution, LF - grain boundary density); $\omega_0 = 2\pi f_0$, the frequency at the peak of the semicircle, knowing R, allows for determination of the capacitance via $\omega_0.R.C = 1$ [77, 78]. Experimentally, the impedance spectroscopy data are collected in samples with metallic electrodes (Au, Ag, Pt or other metals, depending on the charge carrier and measuring temperature) usually in a parallel plate capacitor configuration. The choice of metallization can impact the contact resistance and contribute additional R and C components. Three adimensional parameters may be evaluated [79]: the blocking factor $\alpha_R = R_{gb}/(R_g + R_{gb})$ (the fraction of charge carriers that are blocked at the interfaces), the frequency factor $\alpha_f = f_{0gb}/f_{0g}$ (f_{0gb} and f_{0g} are the peak frequencies of the grain boundary (gb) and grain (g) semicircles, respectively), and the capacitance factor $\alpha_C = C_{gb}/C_g$. The blocking factor is proportional to the intergranular area and the frequency factor to the intergranular distance [79], meaning that their product is proportional to the intergranular volume, i.e., in a first approximation, to pore volume [79, 80]. The capacitance factor allows for the evaluation of the pore to grain volume ratio [79].

Accumulation of charged defects in the intergranular region, promoting the blockage of charge carriers during electrical conductivity/resistivity measurements, is known to be responsible for the grain boundary resistance (low frequency semicircle in the impedance diagram). Even highly pure specimens show this resistance, demonstrating that such effects need not depend solely on impurity segregation at the interfaces, but can be due to lattice defect accumulation as well [81–86].

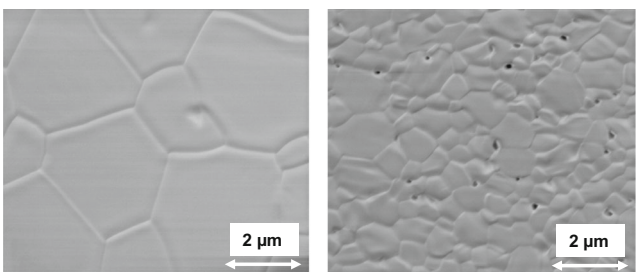

Fig. 1 Typical impedance spectroscopy diagram of an ionic conductor. Z'' - imaginary component; Z' - real component; R - resistance; HF - high frequency (grains); LF - low frequency (interface, mainly grain boundaries); β - depression angle; $\omega_0 = 2\pi f_0$, f_0 - peak frequency

1.3 In situ impedance spectroscopy

In situ impedance spectroscopy consists in collecting impedance data while an experiment is under way and may include simultaneously collecting other data, e.g., laser Raman activity [87]. Simultaneous electrical and dilatometric measurements have already been carried out in solid electrolytes [25], tin dioxide [38, 39], soda-lime glass [88], TiO_2 nanopowders [89] and nanocrystalline CeO_2 [90, 91]. The simultaneous monitoring of the electrical behavior during heating in dilatometric measurements is key for providing additional information on microstructure evolution (grain growth, neck formation between particles, and pore elimination).

In the following, we present the experimental procedures for collecting simultaneously impedance spectroscopy and dilatometric data during electric field-assisted sintering of electroceramics at several temperatures prior to and after electric current flow through the specimens.

2 Experimental

2.1 Electric field-assisted (flash) sintering

Figure 2 is a simplified scheme of time-dependent profiles of temperature, electric field and electric current during an electric field-assisted sintering experiment. AC or DC electric fields can be applied either during heating the specimen (dynamic, Fig. 2a) or at a constant temperature (isothermal, Fig. 2b and c). In the latter, a single electric current pulse or several pulses may be required depending on the shrinkage

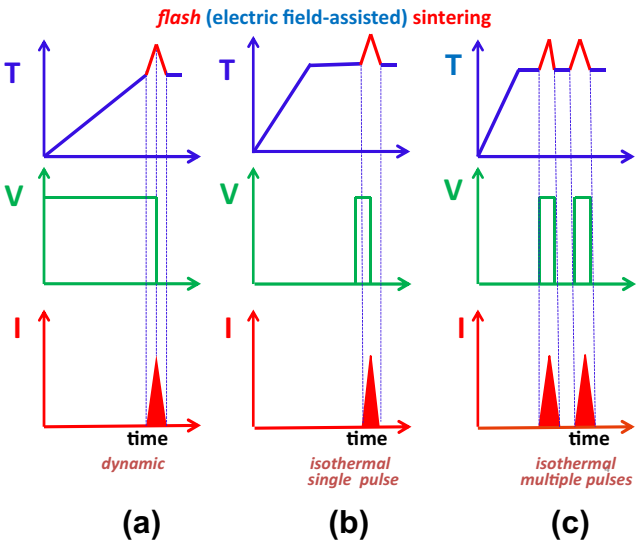

Fig. 2 Scheme of the dependence of temperature, voltage and current during the flash sintering event. **a** during heating - dynamic; **b** single pulse at constant temperature - isothermal; **c** two pulses at constant temperature - isothermal. T: temperature, V: voltage, I: current

level reached by the specimen. Sintering can be achieved in time scale as short as few seconds, then the phenomenon being named "flash sintering", used in this article as one of the methods of the electric field-assisted sintering technique.

Two experimental procedures have been reported for flash sintering:

- First: 1) a green or pre-sintered specimen, usually having a dog-bone shape, is suspended inside a vertical tubular furnace with platinum leads at its extremities, connected to a power supply; 2) an electric voltage is applied either during heating or at a fixed temperature; 3) upon a sudden increase in temperature caused by an up rise in the electric current through the specimen (after a certain time called delay or incubation time) [27], the electric voltage is decreased in order to keep the current constant at a pre-fixed value. The shrinkage of the specimen is monitored with a camera positioned close to one of the apertures of the tubular furnace. Electric voltage, electric current as well as specimen temperature are monitored simultaneously [8].
- Second: 1) a heating rate-dwelling temperature-dwelling time profile is set for a cylindrical green or pre-sintered ceramic pellet positioned inside a vertical dilatometer, with platinum electrodes and terminal leads connecting the parallel surfaces of the specimen to a power supply; 2) an electric field either DC or AC at a chosen frequency is applied to the specimen either upon heating (Fig. 2a) or at the dwelling temperature (Fig. 2b); 3) when the electric current, which flows through the specimen promoting shrinkage, reaches the pre-fixed limiting value, the electric field is turned off and can be re-applied as many times as necessary (Fig. 2c) for the shrinkage level to reach the desired level (followed simultaneously at the dilatometer gauge). Commercial power supplies switch automatically from electric voltage to current control to maintain applied constant power as sample resistance decrease as consequence of the increase in temperature due to Joule heating. In the flash sintering experiments reported by the authors, the power supply switches off when the electric current reaches a pre-set limit value. Afterwards it may be turned on manually. Shrinkage level and sample temperature are monitored with the dilatometer software, while electric field and current are collected in a datalogger. Impedance spectroscopy data are collected before and after the occurrence of the electric current pulses [21].

Figure 3 shows the three applied field-electric current profiles in flash sintering experiments. In one of the experiments (top Figure) an electric current limit is preset and an electric voltage is applied until the current limit is reached, the voltage being then decreased to keep the specimen under the limit current to avoid thermal runaway (continuous increase of the current with consequent increase in temperature due to Joule heating). In another experiment (middle Figure), a voltage is applied at a chosen temperature up to the occurrence of a current pulse, when the voltage is then turned off. In the figure at the bottom, several voltage pulses with the same amplitude are turned on and off, promoting electric current pulses to reach a pre-determined shrinkage level, which could be followed in a dilatometer.

2.2 DC and AC electric fields

DC and AC electric fields have been applied during flash sintering experiments. An equivalence between both has been reported on experiments on 3YSZ [26], but the experiments were limited only to DC and 60 Hz frequency. The obvious difference between DC and AC stems from the fact that DC fields promote charge and mass transfer in the zirconia-based solid electrolytes while AC fields transport only charges. The electrochemical behavior of zirconia polycrystalline specimens is not detected by many authors because the electric current pulses leading to flash sintering have short times (seconds) with no noticeable experimental effect (like the so called blackening of zirconia [92, 93]), because the diffusion of oxide ions is strongly dependent on the temperature (Boltzmann factor) and weakly dependent on time ($t^{1/2}$). Moreover, enhanced grain growth on the cathode side of 8YSZ under a DC electric field, leading to microstructural inhomogeneity, was reported [94].

An experimental evidence of the dependence of the flash sintering on the frequency of the AC electric field was described by evaluating shrinkage, microstructure and impedance spectroscopy data of similar YSZ specimens flash sintered under the same conditions (sample size, shape and green density, temperature, electric power, current limit) but under AC fields with frequencies of 500 Hz, 750 Hz and 1000 Hz [95]. Similar results have been obtained in scandia-stabilized solid electrolytes and a detailed report of these results will be published elsewhere [96]. The attained shrinkage level, the average grain size and the electrical behavior evaluated by impedance spectroscopy showed without doubts that the frequency of the electric field plays an important role in flash sintering experiments.

2.3 Experimental setup

Figure 4 is a schematic view of the experimental arrangement for simultaneous measurement of shrinkage and electrical behavior of an electroceramic upon heating and cooling. The green or pre-sintered cylindrical sample is positioned inside a Unitherm 1161 Anter vertical dilatometer, with platinum (grids) electrodes on both parallel surfaces and platinum terminal leads connected either to a power supply (custom built 65 V-6A, 0.5–1.1 kHz or a commercial 150 V-20A programmable Pacific Smart Source model 118-ACX) or to an impedance analyzer (Hewlett Packard 4192A - 5 Hz to 13 MHz or

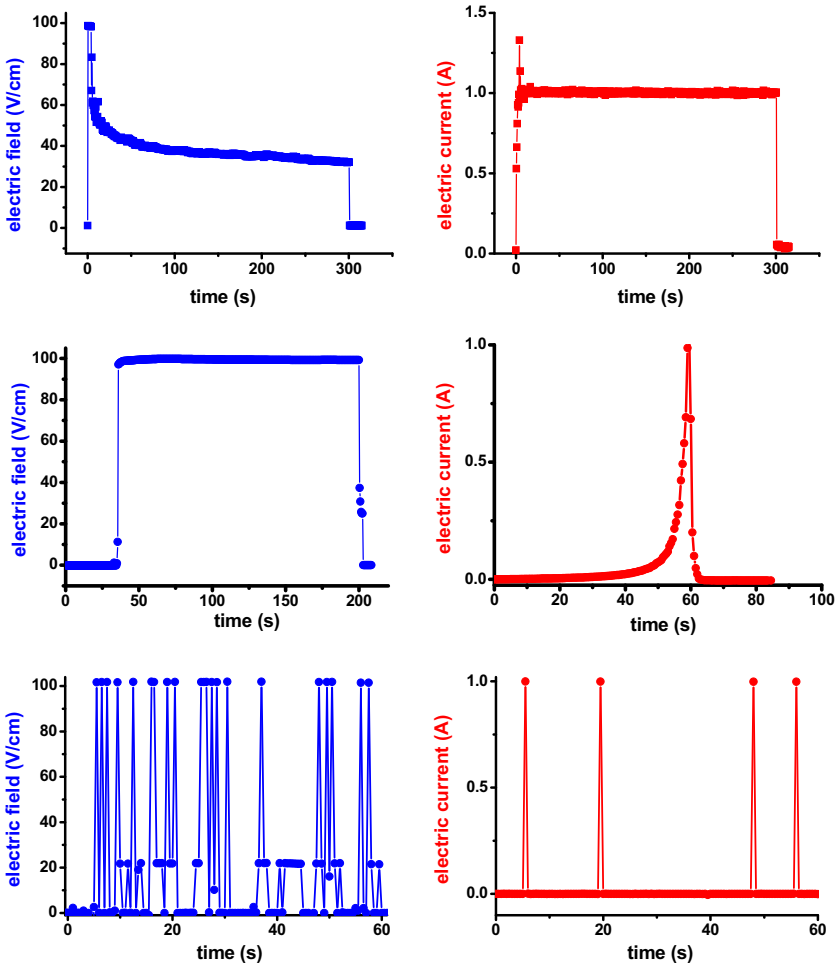

Fig. 3 Electric field and current profiles during flash sintering experiments. Top - the electric field is programmed to decrease to keep constant the current; middle - constant electric field up to a single electric current pulse; bottom - several constant electric field pulses and the corresponding current pulses. See text for details

Agilent 4294–40 Hz to 110 MHz). Shrinkage as a function of temperature is evaluated in the dilatometer and the [−Z"(ω) x Z' (ω)] impedance spectroscopy data are collected in the impedance analyzer *before* the sample is connected to the power supply for application of the electric voltage to produce one or more electric current pulses, and *after* disconnecting the power supply. A full account of the electrical behavior of the specimen is registered during heating up for flash sintering and cooling down the flash-sintered specimen. We must point out that the temperature collected by the dilatometer does not correspond to the actual temperature of the specimen because the Pt-Pt10%Rh type S thermocouple, besides being encapsulated in a closed end alumina tube, is located 5 mm from the specimen position. However, this does not modify the main interpretation of the in situ impedance spectroscopy experimental data.

2.4 Samples

ZrO_2: 8 mol% Y_2O_3 powders (8YSZ, Tosoh, Japan), composed of granules of nanosized particles with 16 ± 3 m^2/g surface area, were uniaxially pressed in cylindrical shape at 10 MPa and isostatically at 200 MPa. The geometrical density was 45%TD (TD: theoretical density). $BaCe_{0.8}Zr_{0.1}Y_{0.1}O_{3-\delta}$ compounds were obtained by solid state reaction by three times calcination at 1250 °C for 16 h with intermediate attrition milling with 3Y–TZP grinding media using stoichiometric amounts of (Alfa Aesar) barium carbonate and cerium, zirconium and yttrium oxides. The attrition milled ceramic powders were pressed to pellets as described above. The geometrical density was in the 35–40 % TD range. Typical dimensions of all pellets were 4.7 mm diameter and 4 mm thickness. Samples of SnO_2 thoroughly mixed to 0.5 wt.% MnO_2 (both Alfa Aesar 99.9 %) were pressed to pellets as described above, achieving ~40 % TD. Chloroform-diluted platinum paste (ESL platinum conductor paste) was deposited on the parallel surfaces of the ceramic green pellets for improving the electric voltage homogeneity through the specimens.

As-sintered lateral surfaces and polished (16, 5, 3 and 1 μm average particle diamond paste) and thermally etched non-metalized parallel surfaces of the electric field-assisted and conventionally sintered specimens were observed in an Inspect F50 FEI FEG-SEM microscope. Some of the YSZ

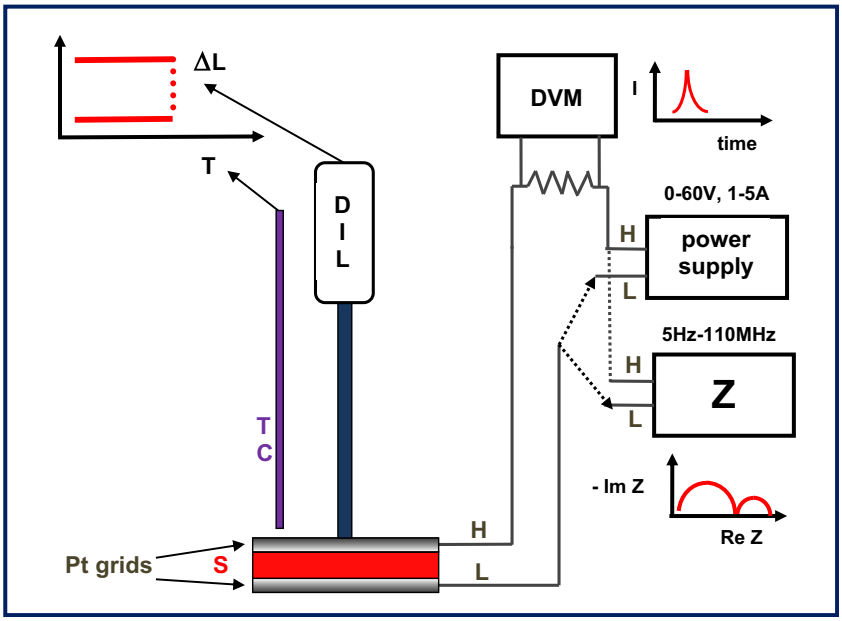

Fig. 4 Experimental setup for dilatometric measurements and simultaneous collection of in situ impedance spectroscopy data before and after electric field-assisted sintering of electroceramics in the room temperature-1500 °C range (isothermal conditions). S - sample; DIL - Unitherm 1161 Anter dilatometer; ΔL - shrinkage; TC - thermocouple; I - electric current; Z - Hewlett Packard 4192A or Agilent 4294 impedance analyzers; Re Z and Im Z - real and imaginary components of the impedance, respectively; DVM - digital voltmeter; H and L - Pt leads connecting the Pt grids (sample electrodes) either to the power supply or to the impedance analyzer Z

polished specimens were mounted with Buehler epoxy thermoset and had the Vickers hardness evaluated in a Buehler Macro Vickers 5112 Hardness Tester with 150 N load during 15 s.

3 Results and discussion

3.1 In situ Impedance Spectroscopy & Flash Sintering

Figure 5 shows a dilatometric curve of a ZrO_2: 8 mol% Y_2O_3 ceramic pellet from room temperature to 1400 °C and down to 400 °C with 10 degree/min heating and cooling rates as recorded by the dilatometer, without any correction. The first sintering stage is detected from room temperature to ~1000 °C and the second from that temperature to 1400 °C. The maximum shrinkage reached is ~25 %. Impedance spectroscopy data were collected every 100 degrees from 500 °C up to 1200 °C and from 1200 °C down to 500 °C. The arrows inserted in the Fig. 5a point to the starting temperature the impedance spectroscopy data (Fig. 5b-i) were collected. At 10 degree/min, the deviation in temperature during each measured spans from as low as 1.6 % at 1300 °C to 4 % at 500 °C, being considered negligible. The reduction in the thickness (measured at the dilatometer) was taken into account to correct the impedance spectroscopy data. The impedance plots during heating consist of one semicircle due to bulk and interfaces, mainly pores. However, for the data being collected dynamically during heating or cooling, one must point out that the sample temperature is not constant in its whole volume, modifying the impedance plot mainly at low frequencies. After being heated to 1400 °C, the 8YSZ is sintered with 25 % thickness shrinkage and the bulk semicircle (HF in Fig. 1) is resolved (Figs. 5b to e). In Figs. 5f to i, after heating to 1400 °C, the bulk semicircle in the cooling plots is not seen due to the inductance effect, known to occur in the high frequency and low resistance impedance spectroscopy measurements with the HP 4192A analyzer. The reduction in the resistance is apparently remarkable in the specimens sintered at 1400 °C.

In the sequence, we report in situ impedance spectroscopy measurements in yttria-stabilized zirconia solid electrolytes exposed to electric fields at 1100 °C inside a dilatometer (Cf. Figure 4). The impedance spectroscopy data were collected at 600, 700, 800, 900, 1000 and 1050 °C before and just after the application of 100 V/cm at 1 kHz with a limiting current of 1 A. The longitudinal retraction, promoted by the electric field, achieved at the end of the experiment, is 11.3 %. The primary effect of the electric field is the occurrence of an electric current through the specimen, producing Joule heating at the interfaces. One may speculate that the increase in the local temperature leads to a decrease of the resistivity, an increase in mobility of charged species with consequent accelerate diffusion of charged species, finally promoting shrinkage and densification. The increase of the temperature at the interfaces might also weld the particles with neck formation [12], as evidenced in Figs. 6e to g, where the high frequency (HF = bulk) and the low frequency (LF = grain boundaries)

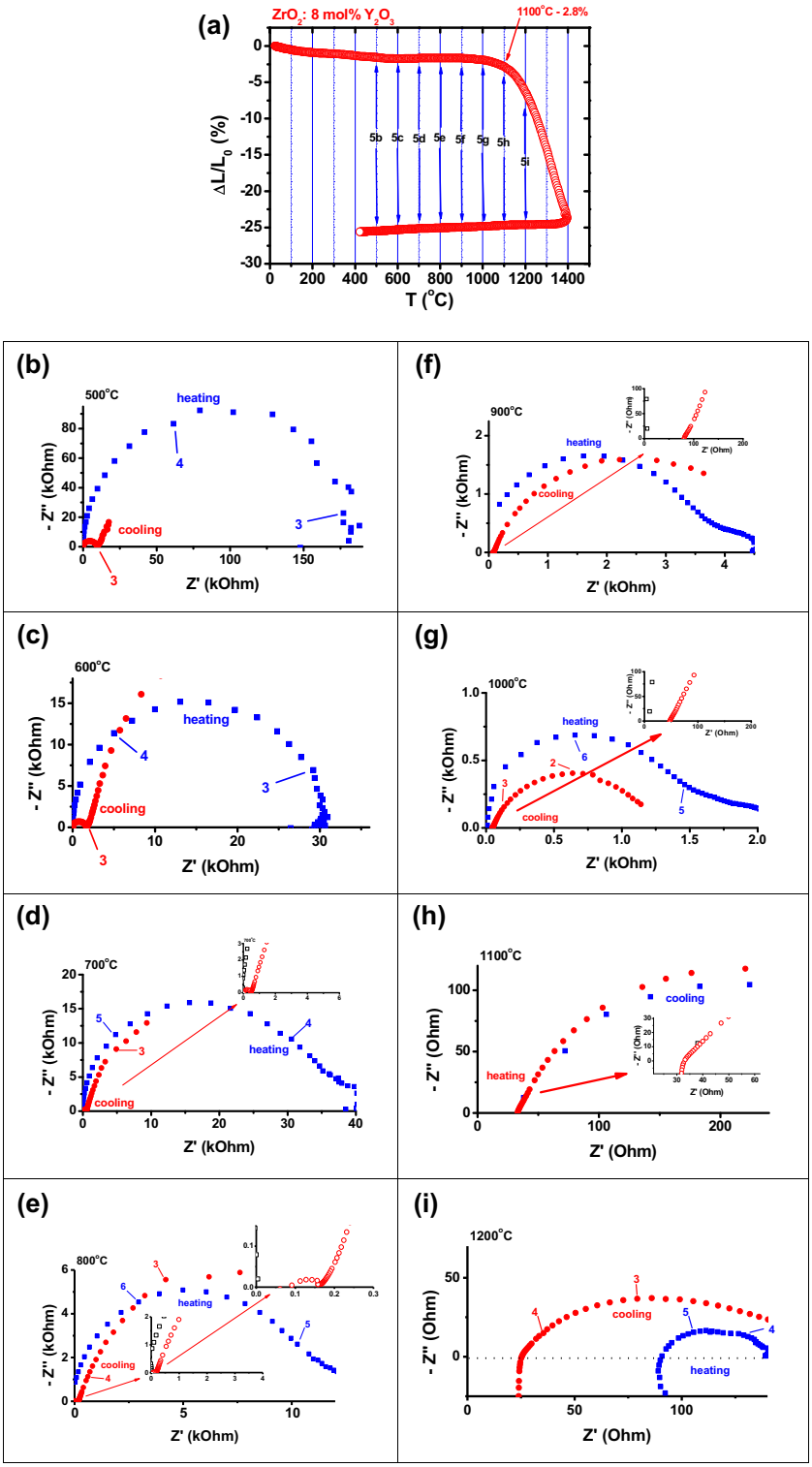

Fig. 5 **a** Dilatometric curve of ZrO_2: 8 mol% Y_2O_3 in the room temperature-1400 °C-400 °C range. The arrows point to the temperatures the impedance data were collected; **b to i**: Impedance spectroscopy diagrams measured at several temperatures from 500 °C to 1200 °C during heating and cooling. Numbers on top of the impedance diagrams stand for log f (f - Hz). Insets in some figures are exploded views of the high frequency region

semicircles are well separated. The associated capacitance values, evaluated in Fig. 6e (diagram on cooling) by the eq. $C = (2.\pi.f_0.R)^{-1}$ (See Fig. 1) yield ~5 × 10^{-7} F and ~8 × 10^{-11} F for the low frequency and the high frequency semicircles, respectively. Those values are typical of grain boundary and bulk capacitances, respectively [97].

Figure 7 shows Bode diagrams of the imaginary component of two impedance diagrams of Fig. 5 (conventionally sintered 8YSZ) and Fig. 6 (flash sintered 8YSZ). It is apparent that the impedance data collected in situ during heating the specimen from room temperature present only one well defined response at 600 °C peaking at 6 × 10^4 Hz while the

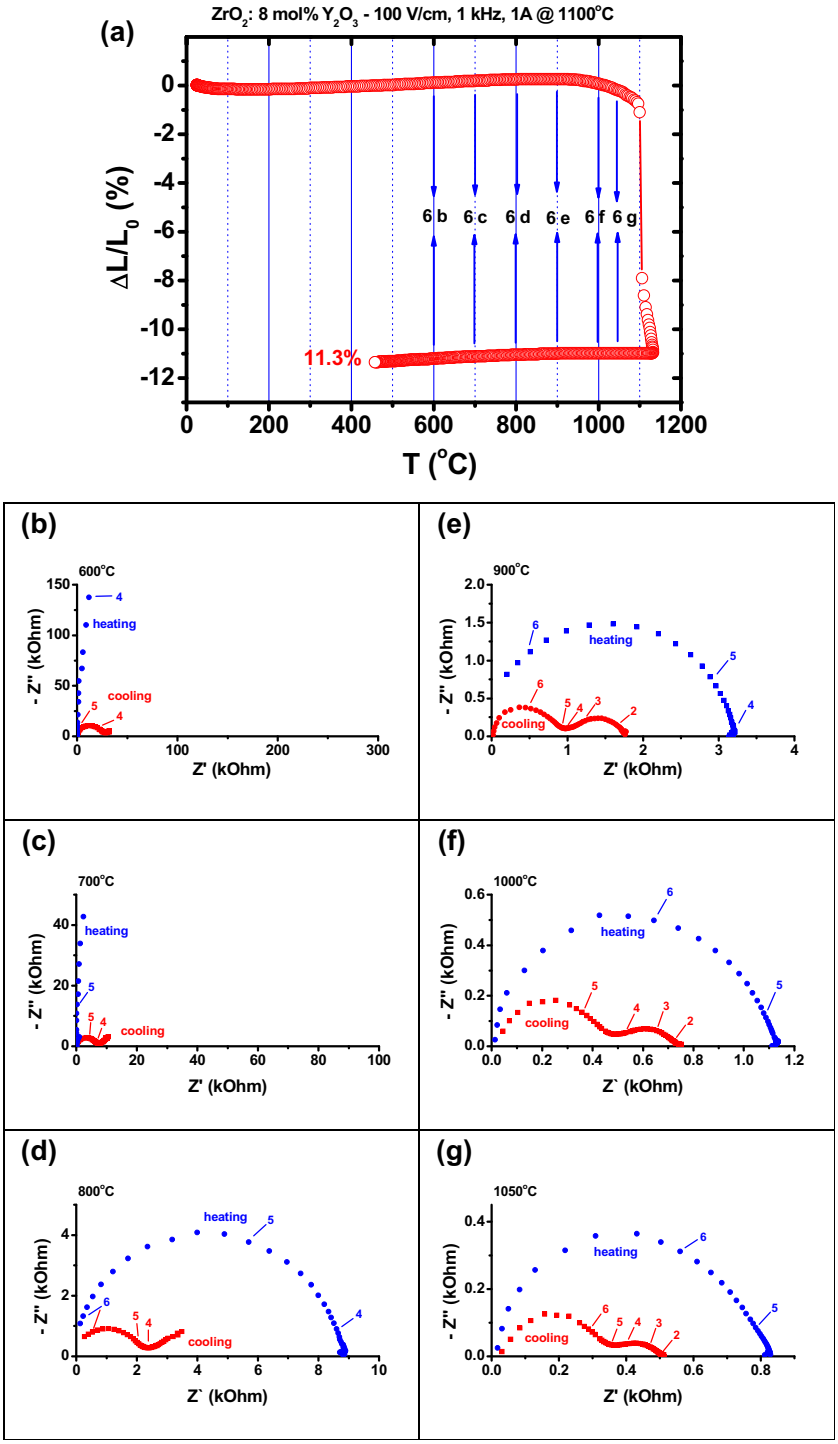

Fig. 6 **a** Dilatometric curve of ZrO_2: 8 mol% Y_2O_3 in the room temperature-1000 °C-450 °C range submitted to 100 V/cm, 1 kHz, 1 A limiting current, at 1100 °C. The arrows point to the temperatures the impedance data were collected; **b to g** impedance spectroscopy diagrams measured at several temperatures from 600 °C to 1050 °C during heating and during cooling after flash sintering. Numbers on top of the impedance diagrams stand for log f (f - Hz)

sintered specimen presents one response at that temperature peaking at 1×10^6 Hz. The flash sintered specimen, on the other hand, besides the only one well-defined response collected at 900 °C upon heating, shows unequivocally two well-defined responses at that temperature during cooling after flash sintering. The first conclusion is that the electric current pulse during the flash sintering experiment provides enough heat to weld the grains (at 1000 °C the 8YSZ particles are already close together) and promote neck formation forming grains and grain boundaries, then the two responses (one due to the bulk with its peak at 1×10^6 Hz and other due to grain boundaries peaking at 400 Hz). Moreover, the 11.3 % shrinkage (Cf. Figure 6a) shows that flash sintering at 1100 °C takes the specimen to the second stage of sintering, where it is known to occur elimination of the majority of porosity, beginning of grain growth and particle coalescence to grains and

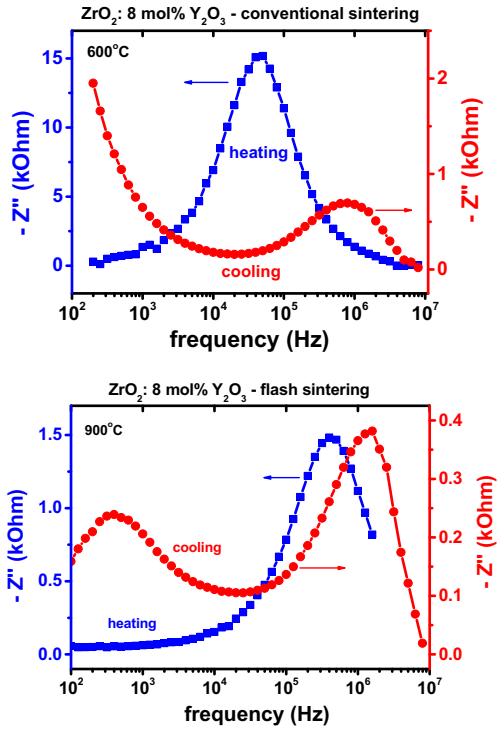

Fig. 7 Bode diagrams of the imaginary component of the impedance of ZrO_2: 8 mol% Y_2O_3 during heating and cooling. Top - at 600 °C, conventional sintering. Bottom - at 900 °C before and after flash sintering at 1100 °C with 100 V/cm, 1 kHz

grain boundaries [1, 2], as confirmed by the two peaks in the Bode diagrams.

The in situ impedance spectroscopy data, either represented by the [−Z“(ω) x Z’(ω)] impedance diagrams or by the [-Z” x log f] Bode diagrams complement the dilatometric data, allowing for the evaluation of grains and grain boundaries upon densification of the ceramic pellet. Moreover, the change in the electrical behavior (one semicircle = one overall electrical response) after application of the electric field (two semicircles = bulk and grain boundary responses) is easily detected. Further, the evolution of the microstructure, with the elimination of porosity, could be followed by deconvolution of the impedance spectroscopy diagrams [98, 99].

The ZrO_2: 8 mol% Y_2O_3 specimens conventionally sintered up to 1400 °C (Fig. 5a) to full density and flash sintered at 1100 °C (Fig. 6a) were inserted together in a sample chamber and had the impedance spectroscopy diagrams measured at 5 temperatures in the 380 - 450 °C range. The [−Z“(ω) x Z’(ω)] impedance spectroscopy diagrams and the corresponding [-Z” x log f] Bode diagrams of the reactance values are exposed in Fig. 8.

The main differences between conventional and flash sintered specimens in Fig. 8 a1-e1 and 8a2-8d2 are: the total resistivity is lower for the conventionally sintered 8YSZ than for the flash sintered specimen because the final shrinkage of the former is 25 % while for the latter is 11.3 %; the same for the grain boundary resistivity due to the smaller average grain size (Cf. Figure 10) with larger blocking surfaces along with pores, additional blockers, in the flash sintered specimen.

Figure 9 shows Arrhenius plots of the grain and grain boundary resistivities, obtained after deconvolution of the impedance diagrams shown in Fig. 8.The bulk values do not differ considerably, meaning that flash sintering at 1100 °C produces samples with the same bulk resistivity as samples sintered at 1400 °C without applying an electric field. The almost one order of magnitude difference in the grain boundary resistivity is due to the larger surface blocking regions as consequence of the significantly small average grain size of flash sintered samples. The activation energies for the bulk (0.81 eV) and the grain boundary (1.03 eV) resistivities are similar to reported values [100].

Figure 10 shows FEG-SEM images of the conventionally and flash sintered 8YSZ specimens both to near full densification.

As expected, and already extensively reported (see Introduction), flash sintered samples have average grain sizes smaller than conventionally sintered samples. One of the reasons is that as densification of 8YSZ happens by interparticle oxide ion diffusion, even though flash sintering times are very short (half-width of the electric current pulse is ~2 s), a large increase in the temperature at the intergranular region enhances diffusion and consequent densification. Diffusion is known to depend weakly on time ($t^{1/2}$) and strongly on temperature ($e^{-H/kT}$, H is the enthalpy and k the Boltzmann constant).

3.2 Shrinkage control by flash sintering

Another interesting aspect of the flash sintering experiments, using the experimental setup sketched in Fig. 4, is the possibility of the application, under isothermal conditions, of multiple electric current pulses (as the power supply turns off the electric field when the electric current reaches the pre-set maximum electric current value, sequential electric fields are manually applied up to the desired shrinkage level), while monitoring at the dilatometer gauge the fraction of the thickness that is reached by the specimen [25]. Figure 11 shows the effect of successive electric current pulses in an 8YSZ ceramic green pellet. The figure shows the reduction of the thickness of ZrO_2:8 mol% Y_2O_3 ceramic pellets to achieve the same density obtained after sintering at 1500 °C (nearly 100 % of the theoretical density), applying many electric current pulses with an electric field of 100 V/cm, 1 kHz, at 800 °C, 1 A maximum electric current. A dilatometric curve of a similar specimen conventionally sintered to full density, heating up to 1500 °C, is also shown.

The final shrinkage in both pellets is 22.5 %. Similar results have already been reported by the authors [25], showing that

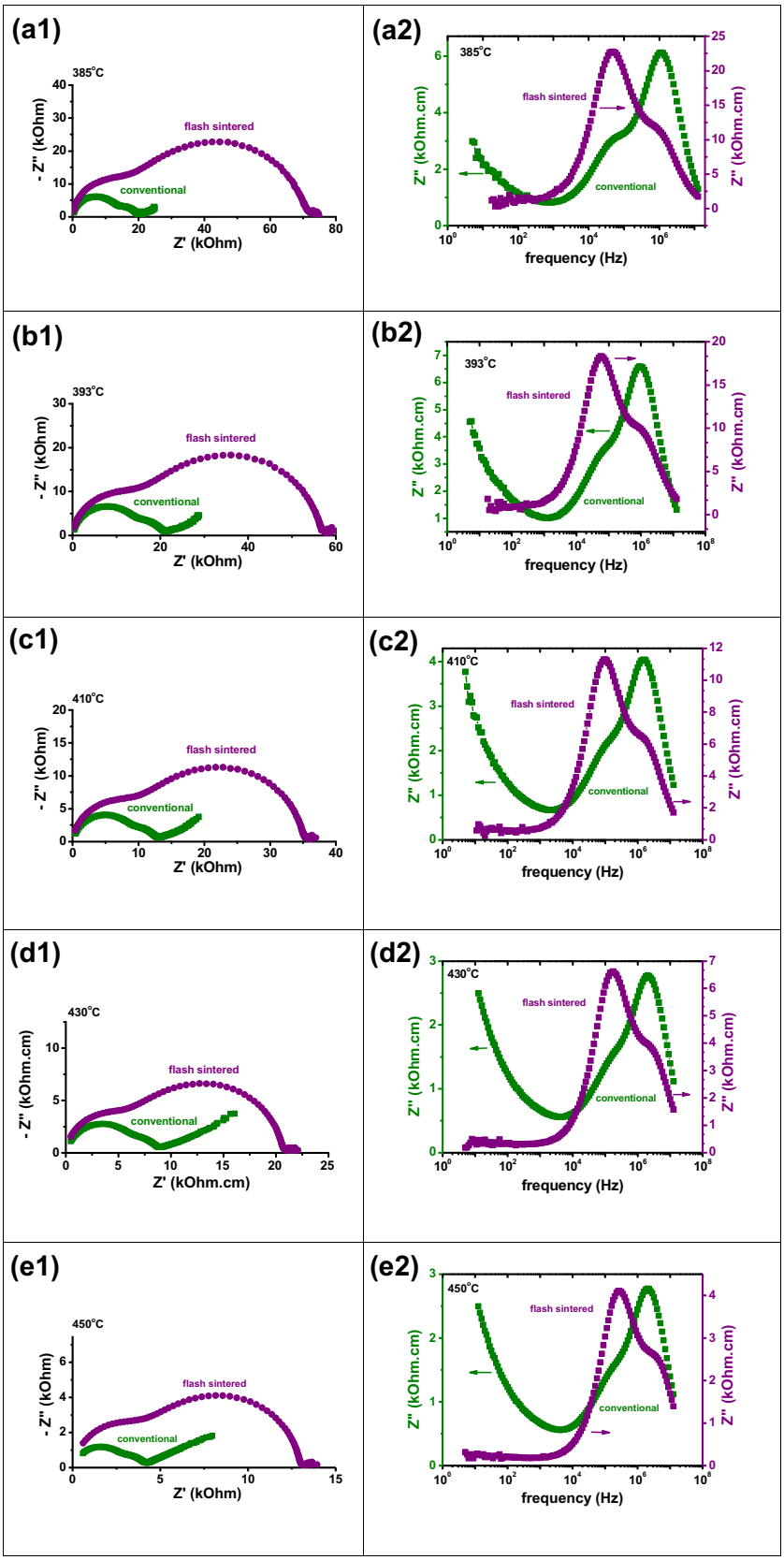

Fig. 8 Left: impedance spectroscopy diagrams measured in ZrO_2: 8 mol%Y_2O_3 at several temperatures after conventional and flash sintering. Right: corresponding Bode diagrams

at any shrinkage level taking the sample to the second sintering stage, its microstructure consists of fine grains and high intergranular electrical resistance, ascertained by impedance spectroscopy measurements.

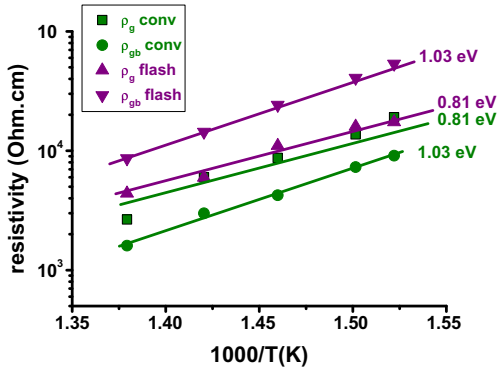

Fig. 9 Arrhenius plot of the resistivity of grain and grain boundary components of the total resistivity of ZrO_2: 8 mol% Y_2O_3. ρ - resistivity; g - grain; gb - grain boundary; conv - conventional sintering; flash - flash sintering

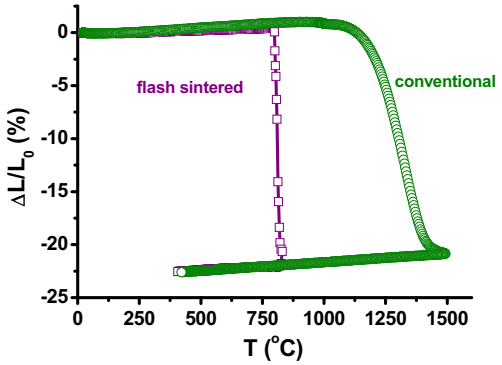

Fig. 11 Dilatometric curves of ZrO_2: 8 mol% Y_2O_3 ceramic pellets in the room temperature-1500 °C-400 °C range, heating rate 10 °C/min (conventional) and in the room temperature-800 °C-400 °C range, heating rate 10 °C/min with application of electric field of 100 V/cm, 1 kHz, 1 A limiting current, at 800 °C

Figure 12 shows the results of another example of controlling the shrinkage level of a ZrO_2: 8 mol% Y_2O_3 ceramic pellet: when the sample reaches 1000 °C, 100 V/cm is applied, enabling sequential electric current pulses to shrink it to a shrinkage level corresponding to the second stage of sintering (~18 %). The electric field is turned off and the heating of the pellet inside the dilatometer continues to 1500 °C, being then cooled down to 400 °C. The same figure shows also the conventional sintering to 1500 °C of a similar sample. The main conclusion is that flash sintering allows for reaching further sintering stages at lower temperatures, by applying an electric field.

After stopping the electric current pulses by turning off the electric voltage when the shrinkage level reaches a value corresponding to the second stage of sintering (for example 18 % in Fig. 12), increasing the temperature of the dilatometer from 1000 °C to ~1200 °C does not modify the value in the dilatometer gauge, increasing afterwards to the same value achieved at 1500 °C in the conventional sintering experiment.

Scanning electron microscopy images of surfaces of the ZrO_2: 8 mol% Y_2O_3 ceramic pellets after conventional sintering at 1500 °C and flash sintering at 800 °C (See Fig. 11), both to full density, are presented in Fig. 13 (a - conventional, b - flash sintered). The average grain size is considerable lower in flash sintered samples, as previously reported in several papers [8, 9, 11, 12, 18, 21, 25].

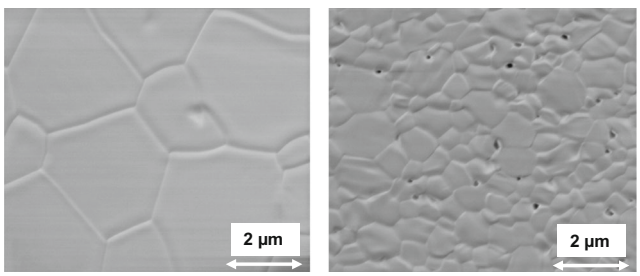

Fig. 10 Scanning electron microscopy micrographs of conventionally sintered (left) and flash sintered (right) ZrO_2: 8 mol% Y_2O_3

3.3 Other electroceramics

In situ impedance spectroscopy measurements were also carried out in other electroceramics to evaluate the extension of the technique to electroceramics with different electrical behavior: a proton conductor and a semiconductor.

3.3.1 Barium cerate zirconate proton conductor

Figure 14 shows dilatometric curve of a $BaCe_{0.8}Zr_{0.1}Y_{0.1}O_{3-\delta}$ ceramic pellet from room temperature to ~1200 °C, being submitted at that temperature to 120 V/cm, 1 kHz, 5 A limiting electric current, during 3 min (Fig. 14a). A huge longitudinal shrinkage is detected. Impedance spectroscopy data were collected at several temperatures before and after the flash sintering (Fig. 14b to g).

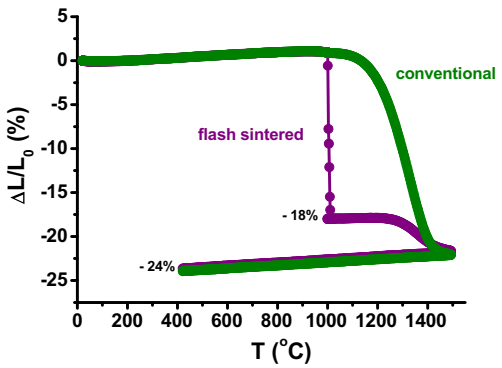

Fig. 12 Dilatometric curves of ZrO_2: 8 mol% Y_2O_3 ceramic pellets in the room temperature-1500 °C-400 °C range, heating rate 10 °C/min (conventional) and with application of 100 V/cm electric field, 1 kHz, 1 A limiting current, at 1000 °C, with subsequent heating to 1500 °C with the electric field turned off

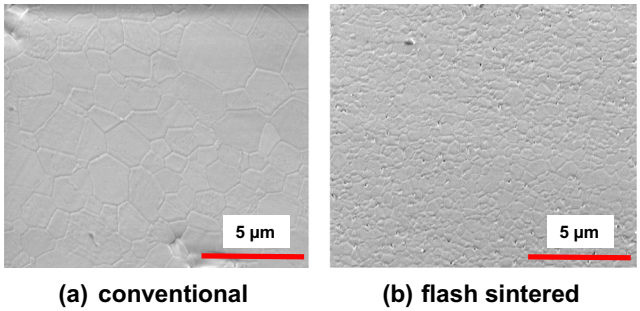

Fig. 13 Scanning electron microscopy micrographs of surfaces of ZrO_2: 8 mol% Y_2O_3 ceramic pellets sintered to full density conventionally at 1500 °C and by flash sintering at 800 °C

The in situ impedance diagrams measured during heating up the BCZY sample inside the dilatometer are composed of just one semicircle due to the electrical resistivity of bulk and interfaces (mainly pores). It is a (resistance//capacitor)-like impedance diagram. After flash sintering, with an impressive ~40 % longitudinal shrinkage, a very large reduction in the electrical resistance is attained: 5.6 to 0.24 kOhm at 1100 °C, 15 to 0.37 kOhm at 1000 °C, 30 to 0.6 kOhm at 900 °C, etc. One may conclude that, similarly to what happens to the 8YSZ oxide ion conducting solid electrolyte, the primary consequence of the electric current pulses produced by the electric field is inter-particle Joule heating to temperatures high

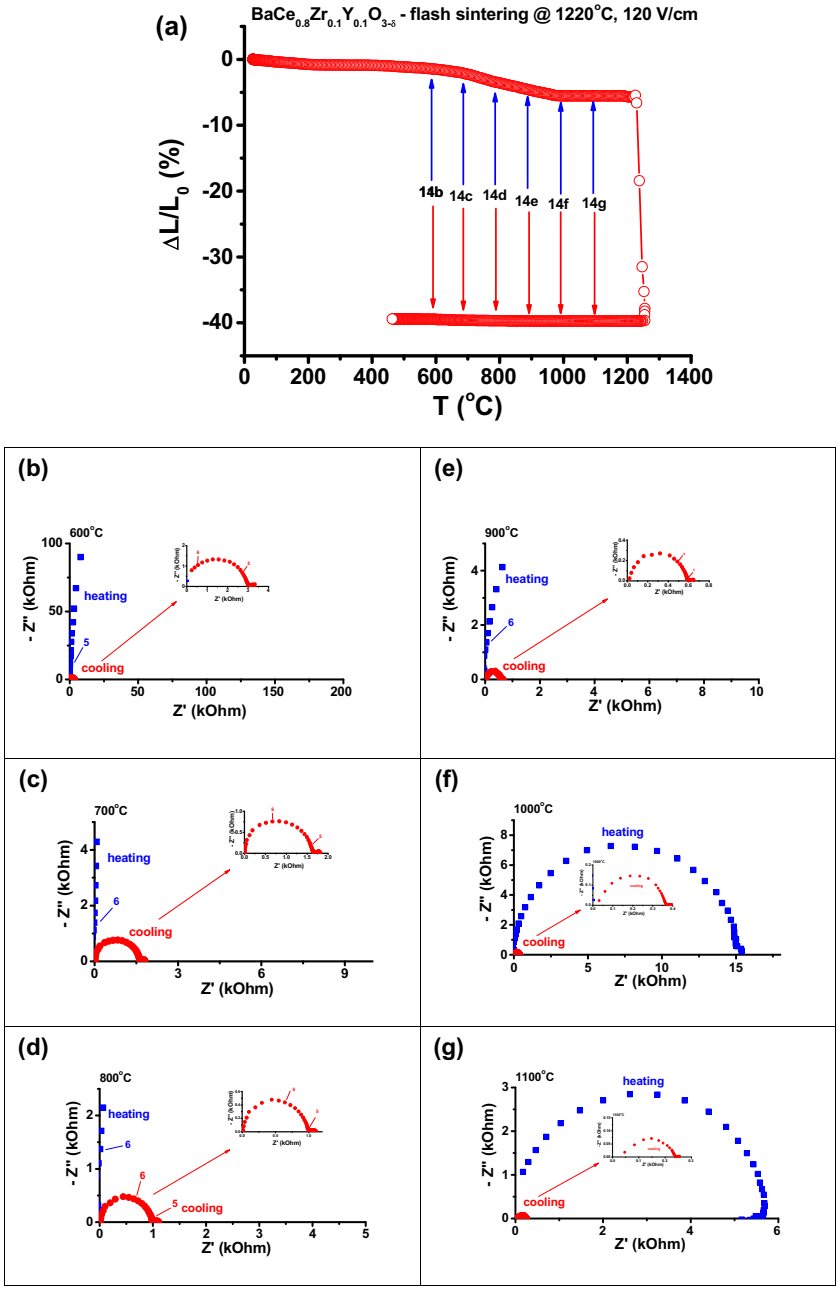

Fig. 14 **a** Dilatometric curve of $BaCe_{0.8}Zr_{0.1}Y_{0.1}O_{3-\delta}$ in the room temperature-1220 °C-450 °C range submitted to 120 V/cm, 1 kHz, 5 A limiting current, at 1220 °C. The arrows point to the temperatures the impedance data were collected; **b to g** impedance spectroscopy diagrams measured at several temperatures from 600 °C to 1100 °C during heating and during cooling after flash sintering. Numbers on top of the impedance diagrams stand for log f (f - Hz). Insets in some figures are exploded views of the high frequency region

enough to promote sintering by joining particles to form grains and welding the grains to consolidate the pellet. It is important to emphasize, at this point, that solid electrolytes flash sintered to nearly full density apparently do not present the usual grain and grain boundary responses to the electric resistivity in the impedance diagrams (Cf. Figure 1). It looks like the passage of an electric current pulse at the interfaces facilitates somehow the grain-to-grain transport of charge carriers (see below the mechanisms section).

3.3.2 Tin dioxide semiconductor

Pure SnO_2 is a semiconductor known to decompose upon heating, being mixed to other oxides to allow for densification. Flash sintering of SnO_2 and of SnO_2 mixed to different amounts of MnO_2 was already reported by the authors [38, 39]. Here we present in situ impedance spectroscopy measurements before and after flash sintering SnO_2 with 0.5 mol% MnO_2 addition.

Figure 15 shows the dilatometric curve of SnO_2: 0.5 mol% MnO_2 green pellets flash sintered at 1100 °C by applying 100 V/cm, 1 kHz, limiting current 5 A, during 5 min (Fig. 15a). The shrinkage curve is similar to the ones measured in 8YSZ (See Fig. 6a): after the first electric current pulses, besides the huge longitudinal shrinkage, the temperature of the sample increases (at constant furnace temperature) due to Joule heating. Impedance plots, collected at several temperatures before and after the application of the AC electric voltage are plotted in Fig. 15b to g. Being a n-type semiconductor, a single semicircle is detected because there is no blocking of electrons at the interfaces. In an ionic conductor, where grains and grain boundaries take part in the resistive process and pores are responsible for increase of the ionic resistivity, the larger is the temperature the specimens are heated, the lower is the ionic resistivity. In a semiconductor, tin dioxide for example, pores act as additional paths for charge carriers, namely, porous specimens present lower electrical resistivity (Fig. 15c to g).

During heating the SnO_2: 0.5 mol% MnO_2 green pellet, the impedance diagrams consist of just one semicircle because the packed particles behave like a R//C component. The same happens after flash sintering at 1100 °C with a reduction of ~11.5 % of the thickness. At high temperatures, the semicircle does not cross the origin of the real axis at high frequencies due to the inductance effect known to occur with impedance analyzers at the high frequencies-low resistance measurements. While 8YSZ and BCZY solid electrolytes have their total resistivity strongly decreased after being submitted to the electric field (flash sintering), the total resistivity increases in flash sintered SnO_2: 0.5 mol% MnO_2. The plausible explanation is that in the former there is a decrease of the blocking of oxide ions at the interfaces while in the latter the pathway for the electrons decreases due to elimination of the easy path through pores.

Figure 16 shows scanning electron microscopy images of lateral non-polished surfaces of SnO_2: 0.5 mol% MnO_2 after heating up to 1100 °C (left) and after flash sintering at 1100 °C by applying 100 V/cm, 1 kHz, 5 A limiting current (right, see also Fig. 15a). While in the former the average grain size is in the submicron range, in the latter, relatively very large grains are observed. This means that heating, due to the electric current pulses crossing the specimen, promotes sintering eliminating pores, and grain growth.

One attempt to explain why flash sintering inhibits grain growth in an ionic conductor and it does not in an electronic conductor: the electric current pulse with the huge increase of the temperature at the intergranular region in few seconds does not change the main sintering mechanism of either 8YSZ or tin dioxide, but enhances the sintering kinetics. The mechanisms governing sintering these oxides are different: in 8YZ it is a densifying mechanism (via lattice or grain boundary diffusion) while in SnO_2 it promotes coarsening (evaporation condensation mechanism) and some degree of densification due to manganese dioxide addition.

3.4 Flash Sintering & Mechanical Properties

Besides sintering yttria-stabilized zirconia to full density at temperatures well below the conventional ones, inhibition of grain growth due to the short elapsed time of the current flash through the ceramic sample has been reported [21]. Ceramic samples with small average grain size usually present enhanced mechanical strength whether there is a good bonding between the different ceramic grain boundaries [101]. The question is how a process as fast as flash sintering could generate strong bond between grains. The impedance spectroscopy plots in flash sintered 8YSZ, consisting of bulk and grain boundary responses are indirect evidence that grains have been welded [12]. As a direct evidence is required, hardness Vickers (HV) experiments were carried out on 8YSZ flash sintered to 25 % and to 100 % final shrinkage level: the values for HV were 540 and 1230 for the 25 % and for the 100 % sample, respectively. The value for the 100 % sample is close to the value reported for the commercial sample (1250) [102]. In Fig. 17 two images of the indentation profile, taken in a FEG-SEM, are shown. It is evident the larger damage (and consequently the lower fracture toughness) in the 25 % flash sintered sample in comparison to the 100 % sample.

3.5 Flash sintering mechanisms

Based on experimental results on the application of the flash sintering technique to several electroceramics, many attempts to explain short time sintering without considerable grain growth have been reported [70]. Evidently, the first

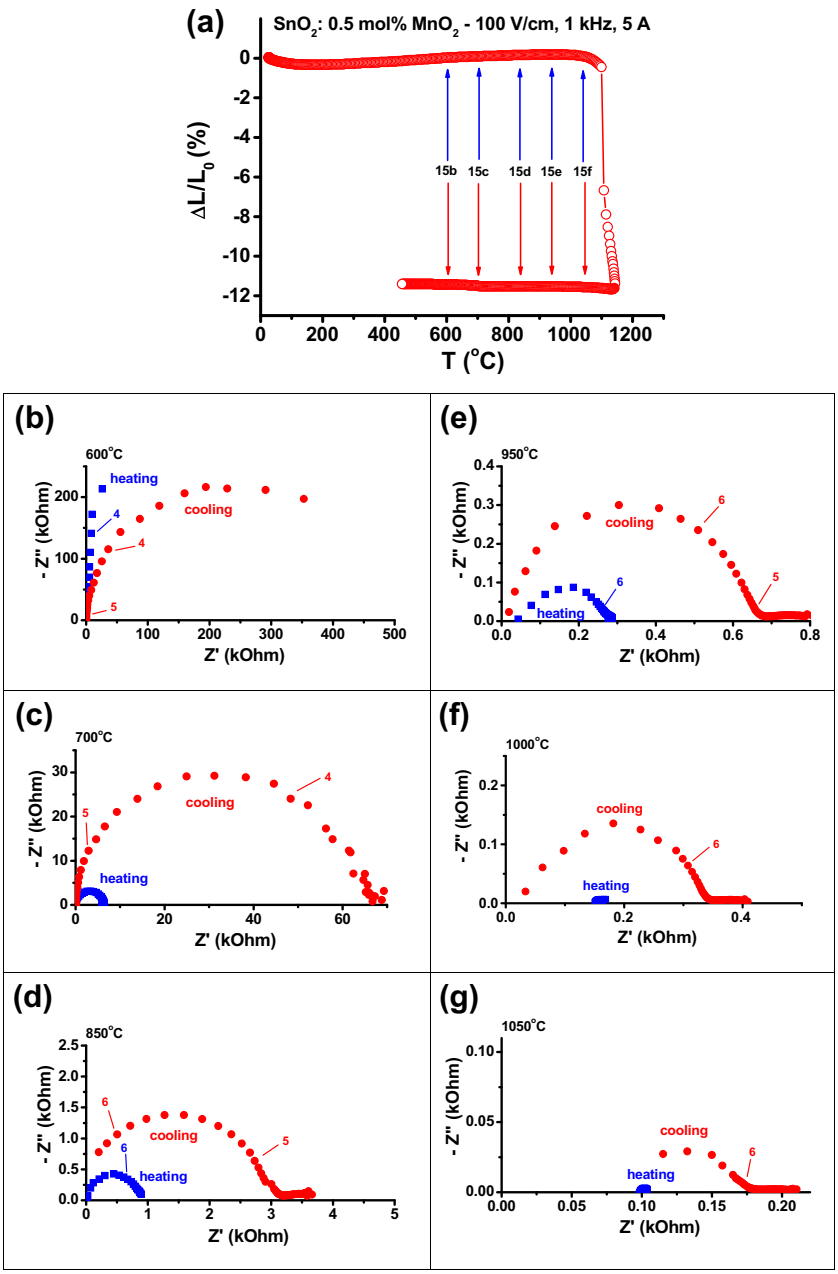

Fig. 15 **a** Dilatometric curve of SnO_2: 0.5 mol% MnO_2 in the room temperature-1100 °C-450 °C range submitted to 100 V/cm, 1 kHz, 1 A limiting current, at 1100 °C. The arrows point to the temperature the impedance data were collected; **b to g** impedance spectroscopy diagrams measured at several temperatures during heating (up in the figures) before and cooling (down) after flash sintering. Numbers on top of the impedance diagrams stand for log f (f - Hz)

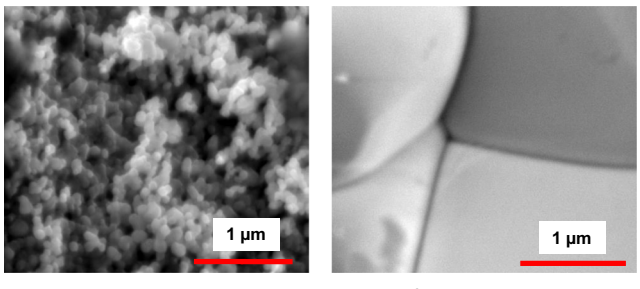

Fig. 16 Scanning electron microscopy micrographs of surfaces of SnO_2: 0.5 mol% MnO_2 sintered at 1100 °C (*left*) and flash sintered at 1100 °C with 100 V/cm, 1 kHz, 5 A limiting current (*right*)

consequence of applying an electric field to a ceramic piece under heating or at a fixed temperature, besides electric polarization, is the electric current through the specimen, which, by its turn, promotes Joule heating. Joule heating is then the primary effect, increasing the temperature in the electric current pathway. Attention has not been paid for looking the possible pathways, which could be the particle (or grain) interfaces or even the actual particle (or grain). The answer is not trivial, because it depends on the temperature the electric pulse occurs, and on the electrical behavior of the electroceramic at that temperature (the same question still remains for the charge carriers responsible for the Joule heating). Mechanisms based on defect formation with enhanced vacancy diffusion and

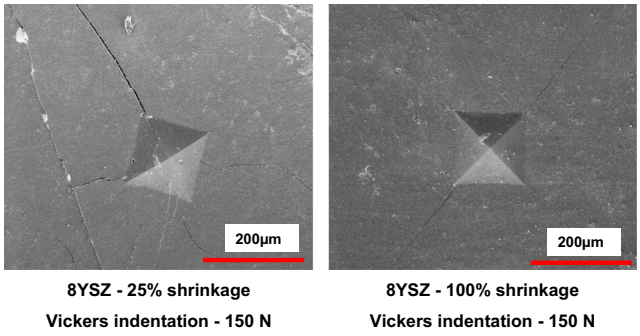

Fig. 17 Scanning electron microscopy micrographs of ZrO_2: 8 mol% Y_2O_3 flash sintered up to 25 % (*left*) and 100 % (*right*) of the maximum shrinkage after indentation with 150 N load for Vickers hardness evaluation

estimates of the local temperature by the black body radiation using the Stefan-Boltzmann law were proposed [70, 71].

Our results on impedance spectroscopy measurements after flash sintering ZrO_2: 8 mol% Y_2O_3 oxide ion conductor to nearly full density show that apparently there is no grain boundary semicircle in the impedance plot. Figure 18 shows impedance diagrams of flash-sintered (18a) and conventionally sintered (18b) to near full density ZrO_2: 8 mol% Y_2O_3, without any normalization respect to the dimensions of the samples. While the specimen fully sintered conventionally (right figure) presents two semicircles due to grains and to grain boundaries, meaning that charge carriers (oxide ion vacancies in 8YSZ) are blocked at the grain boundaries, a similar specimen sintered by the application of the electric field, with observed electric current pulses, shows only one well defined semicircle at high frequencies due to the grains, and a 45° spike at low frequencies. The low frequency semicircle due to the blocking effect is negligible. Two are the possible explanations: 1- if it is a siliceous impurity phase located at the interfaces responsible for blocking charge carriers, the electric current pulse act as scavenging factor [82, 103], transferring those impurities to the triple grain junctions, cleaning the inter-grain region for easy flow of the charge carriers; 2- if one considers chemical species, known to constitute the space charge layer region in this solid electrolyte, as the main blocking factor [81–84], they might be wiped out by the passage of the electric current, promoting the welding of the grains and facilitating charge transfer across the grain boundaries [12]. Moreover, the angular inclination of the low frequency spike suggests a Warburg-like impedance, i.e., diffusion of the charge carriers through the intergranular layer, with negligible blocking (R_{gb} = 0, α_R = 0). Observation of the grain-to-grain region by High Resolution Transmission Electron Microscopy, showing no mismatch, might clear this point.

The effect of localized heating by the flow of an electric current *through the specimen* upon application of an electric field, increasing the temperature at the interfaces of these solid electrolytes, might be responsible for a drastic modification of the space charge region. A schematic representation of this modification is presented in Fig. 19, depicting a decrease of the repulsive potential to the charge carriers, oxide ions, in flash sintered yttria-stabilized zirconia. Before the application of the electric field, top figure, the space charge region consists of "depleted" charge carriers, e.g., oxygen vacancies in the space charge layer of the ZrO_2 grain boundaries [84, 85, 104, 105], CD representing the concentration of oxygen vacancies. After the current pulse(s) due to the application of the electric field, intergranular localized Joule heating occurs, shrinking the specimen with consequent densification and welding the grains; the width δ_{gb} of the space charge region decreases substantially, the amplitude CD of the electric gradient of the locally depleted electric charges decreases, enabling an enhancement of charge carriers diffusion through the intergranular region. Similar phenomenon, not yet verified experimentally, might occur in polycrystalline semiconductors, with their well known Schottky barrier [106].

4 Conclusions and future issues

Conclusions - Electroceramics may have their densification enhanced by application of electric field with production of electric current pulses. The densification to reach a specified shrinkage level occurs at temperatures well below the conventional ones to reach the same level, and grain growth is not as evident in comparison with those achieved in conventional sintering in solid electrolytes. The application of the electric field in the first stage of sintering of yttria-stabilized zirconia,

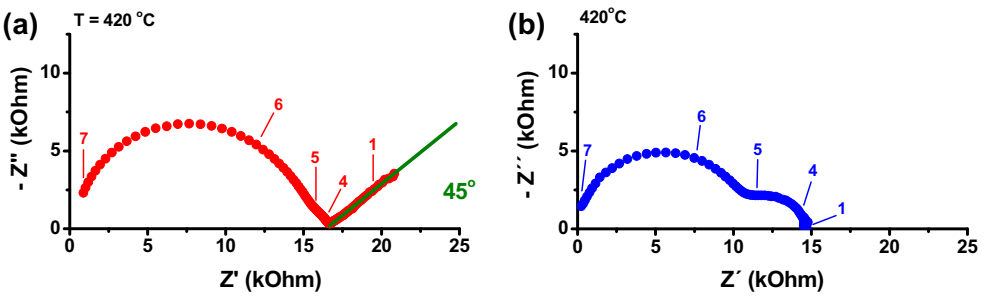

Fig. 18 Impedance spectroscopy diagrams of ZrO_2: 8 mol% Y_2O_3 flash sintered to full density (*left*) and conventionally sintered to full density (*right*)

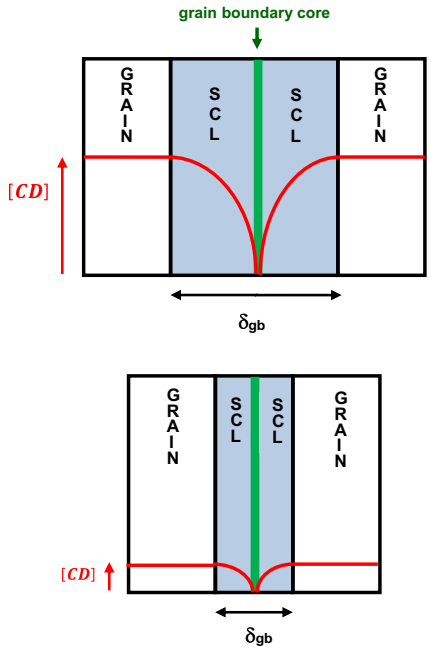

Fig. 19 Simple sketch of the space charge region of thickness δ_{gb} before (*top*) and after (*bottom*) the application of an electric field in a ceramic oxide. SCL: Space Charge Layer; CD: charged defect - oxygen vacancy

for example, is able to take that electroceramic to the second or even to the third stage of sintering, depending on the strength of the field or the number of electric current pulses. Joule heating is considered to be the primary effect of the electric current pulse(s) through the specimen, leading to temperature increase at the intergranular region, with consequent 1- decrease of the electrical resistance, 2- increase in the mobility of charge carriers (mainly oxide ions), 3- increase in the intergranular defect diffusion, and finally 4- densification in a relatively short time, inhibiting grain growth. In situ impedance spectroscopy is a valuable tool for obtaining intragranular (bulk) and intergranular (mainly grain boundaries and pores) data at every step before and after the application of the electric field during the sintering process. These electrical data proved to be important for considering that the modification in the space charge region plays a key role in the electric field (flash) sintering of ion conductors, as shown in zirconia-based solid electrolytes. The comparison of in situ impedance spectroscopy diagrams measured before and after the occurrence of the electric current pulse shows the bulk and grain boundary modification under the application of the electric field leading to densification. Even though some doubts persist on the mechanisms behind the actual effect of the enhancement of the densification under application of the electric field, the flash sintering technique shows promising features for decreasing the cost of production of dense ceramic pieces with improved electrical and mechanical properties as well as a challenge for researchers on Materials Science and Engineering.

Future Issues - there are plenty of research work on experimental as well as theoretical simulation to be performed on this relatively new field of research, flash sintering of electroceramics: 1- find the dependence of the flash sintering conditions (magnitude, frequency and time duration of the applied electric field, threshold electric current) on the microstructure of the green ceramic body; 2- look for the experimental requirements for producing dense (or porous) ceramic bodies with homogeneous microstructure; 3- collect data on detailed analysis of the infrared, visible and ultraviolet electromagnetic radiation emitted during the electric current pulse through the electroceramic; 4- perform flash sintering experiments under different (reducing and oxidizing) conditions; 5- carry out in situ experiments with other techniques like Raman laser spectroscopy, Fourier Transform Infrared spectroscopy, high resolution X-ray diffraction, neutron diffraction, four probe electrical conductivity; 6- design of experimental setups for scaling up the successful laboratory experiments to pilot plants or even to the industrial segment; 7- provide laboratory simulation of the experimental requirements for enabling the densification of electroceramics with shapes and sizes other than the simple ones utilized so far. In situ *impedance spectroscopy might be a valuable technique to be performed along with some of these issues.*

Acknowledgments To CNEN, CNPq (Procs. 470952/2013-0 and 303483/2013-0) and FAPESP (Proc. 2013/07296-2) for financial support. To Prof. Michel Kleitz, formerly at Laboratoire d'Électrochimie des Solides de Grenoble, France, for in the past introducing the authors to the area of Electrochemistry of Solids and recently to the Flash Grain Welding idea. To Yamato Miyao for designing and building custom made power supplies. To Yone V. França and Sabrina G.M. Carvalho for technical assistance

References

1. R. M. German, *Sintering Theory and Practice* (Wiley, 1996)ISBN: 978–0–471-05786-4
2. S.-J. L. Kang, *Sintering - Densification, Grain Growth & Microstructure* (Elsevier, 2004)ISBN: 978–0–750-66385-4
3. C. A. Handwerker, J. E. Blendell, W. A. Kaysser, *Foreword, Ceramic Transactions - Sintering of Advanced Ceramics* (The American ceramic society, USA., ISBN: 0–944904–20-31990)
4. J. D. Katz, Microwave sintering of ceramics. Annu Rev Mater Sci **22**, 153 (1992)
5. J. Orru, R. Licheri, A. M. Locci, A. Cincotti, G. Gao, Consolidation synthesis of materials by electric current activated/assisted sintering. Mater Sci Eng R **63**, 127 (2009)
6. S. Grasso, Y. Sakka, G. Maizza, Electric current activated/assisted sintering (ECAS): a review of patents 1906-2008. Sci Technol Adv Mater **10**, 1 (2009)
7. Z. A. Munir, U. Anselmo-Tamburini, The effect of electric field and pressure on the synthesis and consolidation of materials: a review of the spark plasma sintering method. J Mater Sci **41**, 763 (2006)

8. S. Ghosh, A. H. Chokshi, P. Lee, R. Raj, A huge effect of weak dc electrical fields on grain growth in zirconia. J Am Ceram Soc **92**, 1856 (2009)
9. D. Yang, R. Raj, H. Conrad, Enhanced sintering rate of zirconia (3Y-TZP) through the effect of a weak dc electric field on grain growth. J Am Ceram Soc **93**, 2935 (2010)
10. M. Cologna, B. Rashkova, R. Raj, Flash sintering of Nanograin zirconia in <5 s at 850°C. J Am Ceram Soc **93**, 3556 (2010)
11. D. Yang, H. Conrad, Enhanced sintering rate of zirconia (3Y-TZP) by application of a small AC electric field. Scr Mater **63**, 328 (2010)
12. R. Muccillo, M. Kleitz, E. N. S. Muccillo, Flash grain welding in yttria stabilized zirconia. J Eur Ceram Soc **31**, 517 (2011)
13. S. Grasso, Y. Sakka, N. Rendtorff, C. Hu, G. Maizza, H. Borodianska, O. Vasylkiv, Modeling of the temperature distribution of flash sintered zirconia. J Ceram Soc Japan **119**, 144 (2011)
14. M. Cologna, R. Raj, Surface diffusion-controlled neck growth kinetics in early stage sintering of zirconia, with and without applied DC electrical field. J Am Ceram Soc **94**, 391 (2011)
15. M. Cologna, A. L. G. Prette, R. Raj, Flash-sintering of cubic yttria-stabilized zirconia at 750 degrees C for possible use in SOFC manufacturing. J Am Ceram Soc **94**, 316 (2011)
16. J. S. C. Francis, R. Raj, Flash-Sinterforging of Nanograin zirconia: field assisted sintering and Superplasticity. J Am Ceram Soc **95**, 138 (2012)
17. R. Baraki, S. Schwartz, O. Guillon, Effect of electric field/current on sintering of fully stabilized zirconia. J Am Ceram Soc **95**, 75 (2012)
18. J. S. C. Francis, M. Cologna, R. Raj, Particle size effects in flash sintering. J Eur Ceram Soc **32**, 3129 (2012)
19. J. Obare, W. D. Griffin, H. Conrad, Effects of heating rate and DC electric field during sintering on the grain size distribution in fully sintered tetragonal zirconia polycrystals stabilized with 3 % molar yttria (3Y-TZP). J Mater Sci **47**, 5141 (2012)
20. A. Cordier, M. Kleitz, M. C. Steil, Welding of yttrium-doped zirconia granules by electric current activated sintering (ECAS): protrusion formation as a possible intermediate step in the consolidation mechanism. J Eur Ceram Soc **32**, 1473 (2012)
21. R. Muccillo, E. N. S. Muccillo, An experimental setup for shrinkage evaluation during electric field-assisted flash sintering: application to yttria-stabilized zirconia. J Eur Ceram Soc **33**, 515 (2013)
22. J. A. Downs, V. M. Sglavo, Electric field assisted sintering of cubic zirconia at 390 degrees C. J Am Ceram Soc **96**, 1342 (2013)
23. J. Park, I.-W. Chen, In situ thermometry measuring temperature flashes exceeding 1,700 degrees C in 8 mol% Y_2O_3-stabilized zirconia under constant-voltage heating. J Am Ceram Soc **96**, 697 (2013)
24. M. C. Steil, D. Marinha, Y. Aman, J. R. C. Gomes, M. Kleitz, From conventional ac flash sintering of YSZ to hyper-flash and double flash. J Eur Ceram Soc **33**, 2093 (2013)
25. R. Muccillo, E. N. S. Muccillo, Shrinkage control of yttria-stabilized zirconia during ac electric field-assisted sintering. J Eur Ceram Soc **34**, 3871 (2014)
26. H. Conrad, J. Wang, Equivalence of AC and DC electric field on retarding grain growth in yttria-stabilized zirconia. Scr Mater **72-73**, 33 (2014)
27. J. S. C. Francis, R. Raj, Influence of the field and the current limit on flash sintering at isothermal furnace temperatures. J Am Ceram Soc **96**, 2754 (2013)
28. J.-C. M'Peko, J. S. C. Francis, R. Raj, Impedance spectroscopy and dielectric properties of flash versus conventionally sintered yttria-doped zirconia electroceramics viewed at the microstructural level. J Am Ceram Soc **96**, 3760 (2013)
29. J.-M. Lebrun, R. Raj, A first report of photoemission in experiments related to flash sintering. J Am Ceram Soc **97**, 2427 (2014)
30. R. Muccillo, E. N. S. Muccillo, Light emission during electric field-assisted sintering of electroceramics. J Eur Ceram Soc **35**, 1653 (2014)
31. J. G. P. da Silva, J.-M. Lebrun, H. A. Al-Qureshi, R. Janssen, R. Raj, Temperature distributions during flash sintering of 8 % yttria-stabilized zirconia. J Am Ceram Soc **98**, 3525 (2015)
32. Y. X. Du, A. J. Stevenson, D. Vernat, M. Diaz, D. Marinha, Estimating joule heating and ionic conductivity during flash sintering of 8YSZ. J Eur Ceram Soc **36**, 749 (2016)
33. A. Akbari-Fakhrabadi, R. V. Mangalaraja, F. A. Sanhueza, R. E. Avila, S. Ananthakumar, S. H. Chan, Nanostructured Gd-CeO_2 electrolyte for solid oxide fuel cell by aqueous tape casting. J Power Sources **218**, 307 (2012)
34. X. Hao, Y. Liu, Z. Wang, J. Qiao, K. Sun, A novel sintering method to obtain fully dense gadolinia doped ceria by applying a direct current. J Power Sources **210**, 86 (2012)
35. T. Jiang, Z. Wang, J. Zhang, X. Hao, D. Rooney, Y. Liu, W. Sun, Understanding the Flash Sintering of Rare-Earth-Doped Ceria for Solid Oxide Fuel Cell. J Am Ceram Soc **98**, 1717 (2015)
36. A. L. G. Prette, M. Cologna, V. Sglavo, R. Raj, Flash-sintering of Co_2MnO_4 spinel for solid oxide fuel cell applications. J Power Sources **196**, 2061 (2011)
37. A. Karakuscu, M. Cologna, D. Yarotski, J. Won, J. S. C. Francis, R. Raj, B. P. Uberuaga, Defect structure of flash-sintered strontium Titanate. J Am Ceram Soc **95**, 2531 (2012)
38. R. Muccillo, E. N. S. Muccillo, Electric field-assisted flash sintering of tin dioxide. J Eur Ceram Soc **34**, 915 (2014)
39. E. N. S. Muccillo, R. Muccillo, Electric field-assisted sintering of tin dioxide with manganese dioxide addition. J Eur Ceram Soc **34**, 3699 (2014)
40. E. Zapata-Solvas, S. Bonilla, P. R. Wilshaw, R. I. Todd, Preliminary investigation of flash sintering of SiC. J Eur Ceram Soc **33**, 2811 (2013)
41. S. K. Jha, R. Raj, The effect of electric field on sintering and electrical conductivity of titania. J Am Ceram Soc **97**, 527 (2014)
42. S. K. Jha, J. M. Lebrun, K. C. Seymour, W. M. Kriven, R. Raj, Electric field induced texture in titania during experiments related to flash sintering. J Eur Ceram Soc **36**, 257 (2016)
43. C. Schmerbauch, J. Gonzalez-Julian, R. Roeder, C. Ronning, O. Guillon, Flash sintering of nanocrystalline zinc oxide and its influence on microstructure and defect formation. J Am Ceram Soc **97**, 1728 (2014)
44. A. Gaur, V. M. Sglavo, Flash-sintering of $MnCo_2O_4$ and its relation to phase stability. J Eur Ceram Soc **34**, 2391 (2014)
45. J.-C. M'Peko, J. S. C. Francis, R. Raj, Field-assisted sintering of undoped $BaTiO_3$: microstructure evolution and dielectric permittivity. J Eur Ceram Soc **34**, 3655 (2014)
46. A. Uehashi, H. Yoshida, T. Tokunaga, K. Sasaki, T. Yamamoto, Enhancement of sintering rates in $BaTiO_3$by controlling of DC electric current. J. Ceram. Soc. Japan **123**, 465 (2015)
47. N. Shomrat, S. Baltianski, C. A. Randall, Y. Tsur, Flash sintering of potassium-niobate. J Eur Ceram Soc **35**, 2209 (2015)
48. Y. Zhang, J.-Il Jung, J. Luo, thermal runaway, flash sintering and asymmetrical microstructural development of ZnO and ZnO-Bi_2O_3 under direct currents. Acta Mater **94**, 87 (2015)
49. Y. Zhang, J. Luo, Promoting the flash sintering of ZnO in reduced atmospheres to achieve nearly full densities at furnace temperatures of <120 degrees C. Scr Mater **106**, 26 (2015)
50. S. Schwarz, A. M. Thron, J. Rufner, K. van Benthem, O. Guillon, Low temperature sintering of nanocrystalline zinc oxide: effect of heating rate achieved by field assisted sintering/spark plasma sintering. J Am Ceram Soc **95**, 2451 (2012)
51. M. Cologna, J. S. C. Francis, R. Raj, Field assisted and flash sintering of alumina and its relationship to conductivity and MgO-doping. J Eur Ceram Soc **31**, 2827 (2011)

52. H. Yoshida, Y. Sakka, T. Yamamoto, J. M. Lebrun, R. Raj, Densification behavior and microstructural development in undoped yttria by flash sintering. J Eur Ceram Soc **34**, 991 (2014)
53. E. Champion, Sintering of calcium phosphate bioceramics. Acta Biomater **9**, 5855 (2013)
54. S. Grasso, T. Saunders, H. Porwall, O. Cedillos-Barraza, D. D. Jayaseelan, W. E. Lee, M. J. Reece, Flash spark plasma sintering (FSPS) of pure ZrB_2. J Am Ceram Soc **97**, 2405 (2014)
55. R. Muccillo, E. N. S. Muccillo, M. Kleitz, Densification and enhancement of the grain boundary conductivity of gadolinium-doped barium cerate by ultra-fast flash grain welding. J Eur Ceram Soc **32**, 2311 (2012)
56. T. Jiang, Y. Liu, Z. Wang, W. Sun, J. Qiao, K. Sun, An improved direct current sintering technique for proton conductor - $BaZr_{0.1}Ce_{0.7}Y_{0.1}Yb_{0.1}O_3$: The effect of direct current on sintering process. J Power Sources **248**, 70 (2014)
57. K. S. Naik, V. M. Sglavo, R. Raj, Field assisted sintering of ceramic constituted by alumina and yttria stabilized zirconia. J Eur Ceram Soc **34**, 2435 (2014)
58. A. Gaur, V. M. Sglavo, Flash sintering of (La, Sr)(Co, Fe)O_3-Gd-doped CeO_2 composite. J Am Ceram Soc **98**, 1747 (2015)
59. E. Bichaud, J. M. Chaix, C. Carry, M. Kleitz, M. C. Steil, Flash sintering incubation in Al_2O_3/TZP composites. J Eur Ceram Soc **35**, 2587 (2015)
60. S. K. Jha, J. M. Lebrun, R. Raj, Phase transformation in the alumina-titania system during flash sintering experiments. J Eur Ceram Soc **36**, 733 (2016)
61. Y. Liu, X. Hao, Z. Wang, J. Wang, J. Qiao, Y. Yan, K. Sun, A newly-developed effective direct current assisted sintering technique for electrolyte film densification of anode-supported solid oxide fuel cells. J Power Sources **215**, 296 (2012)
62. D. Liu, Y. Gao, J. Liu, F. Liu, K. Li, H. Su, Y. Wang, L. An, Preparation of Al_2O_3-$Y_3Al_5O_{12}$-ZrO_2 eutectic ceramic by flash sintering. Scr Mater **114**, 108 (2016)
63. J. S. C. Francis, M. Cologna, D. Montinaro, R. Raj, Flash sintering of anode-electrolyte multilayers for SOFC applications. J Am Ceram Soc **96**, 1352 (2013)
64. A. Gaur, V. M. Sglavo, Densification of $La_{0.6}Sr_{0.4}Co_{0.2}Fe_{0.8}O_3$ ceramic by flash sintering at temperature less than 100 degrees C. J Mater Sci **49**, 6321 (2014)
65. L. B. Caliman, R. Bouchet, D. Gouvea, P. Soudant, M. C. Steil, Flash sintering of ionic conductors: the need of a reversible electrochemical reaction. J Eur Ceram Soc **36**, 1253 (2016)
66. O. Vasilkiv, H, Borodianska, Y. Sakka, D. Demirskyi, Flash spark plasma sintering of ultrafine yttria-stabilized zirconia ceramics, Scripta Mater. 121, 32 (2016)
67. S. Grasso, T. Saunders, H. Porwal, B. Milson, A. Tudball, M. Reece, Flash spark plasma sintering (FSPS) of α and β SiC. J Am Ceram Soc **99**, 1534 (2016)
68. S. Grasso, E.-Y. Kim, T. Saunders, M. Yu, A. Tudball, S.-H. Choi, M. Reece, Ultra-rapid crystal growth of textured SiC using flash spark plasma sintering route. Cryst Growth Des **16**, 2317 (2016)
69. B. Niu, F. Zhang, W. J. Zhang, W. Wang, Z. Fu, Ultra-fast densification of boron carbide by flash spark plasma sintering. Scr Mater **116**, 127 (2016)
70. R. Raj, M. Cologna, J. S. C. Francis, Influence of externally imposed and internally generated electrical fields on grain growth, diffusional creep, sintering and related phenomena in ceramics. J Am Ceram Soc **94**, 1941 (2011)
71. R. Raj, Joule heating during flash sintering. J Eur Ceram Soc **32**, 2293 (2012)
72. Y. H. Dong, I. W. Chen, Predicting the onset of flash sintering. J Am Ceram Soc **98**, 2333 (2015)
73. K. S. Naik, V. M. Sglavo, R. Raj, Flash sintering as a nucleation phenomenon and a model thereof. J Eur Ceram Soc **34**, 4063 (2014)
74. R. I. Todd, E. Zapata-Solvas, R. S. Bonilla, T. Sneddon, P. R. Wilshaw, Electrical characteristics of flash sintering: thermal runaway of joule heating. J Eur Ceram Soc **35**, 1865 (2015)
75. H. Yoshida, A. Uehashi, T. Tokunaga, K. Sasaki, T. Yamamoto, Formation of grain boundary second phase in $BaTiO_3$ polycrystal under a high DC electric field at elevated temperatures. J. Ceram. Soc. Japan **124**, 388 (2016)
76. Y. Du, A. J. Stevenson, D. Vernat, M. Diaz, D. Marinha, Estimating joule heating and ionic conductivity during flash sintering. J Eur Ceram Soc **36**, 749 (2016)
77. Impedance Spectroscopy, in *Emphasizing solid materials and systems*, ed by J. R. Macdonald. (John Wiley & Sons, 1987) ISBN-13:978–04718311228
78. C. Déportes, M. Duclot, P. Fabry, J. Fouletier, A. Hammou, M. Kleitz, E. Siebert, J. L. Souquet, *Électrochimie des Solides* (Grenoble Sciences, Grenoble, France, 2008), p. 263
79. M. Kleitz, L. Dessemond, M. C. Steil, Model for ion-blocking at internal interfaces in zirconias. Solid State Ionics **75**, 107 (1995)
80. D. Z. de Florio, R. Muccillo, Sintering of zirconia-yttria ceramics by impedance spectroscopy. Solid State Ionics **123**, 301 (1999)
81. J. Maier, Space charge regions in solid two phase systems and their conduction contribution - II contact equilibrium at the Interface of two ionic conductors and the related conductivity effect. Ber Bunsenges Phys Chem **89**, 355 (1985)
82. X. Guo, W. Sigle, J. Fleig, J. Maier, Role of space charge in the grain boundary blocking effect in doped zirconia. Solid State Ionics **154-155**, 555 (2002)
83. I. Lubomirsky, J. Fleig, J. Maier, Modeling of space charge effects in nanocrystalline ceramics: the influence of geometry. J Appl Phys **92**, 6819 (2002)
84. J. Maier, Ionic-conduction in space charge regions. Prog Solid State Chem **23**, 171 (1995)
85. R. Chaim, Activation energy and grain growth in nanocrystallline Y-TZP ceramics. Mater Sci Eng A **486**, 439 (2008)
86. H. L. Tuller, S. R. Bishop, Point defects in oxides: tailoring materials through defect engineering. Annu Rev Mater Res **41**, 369 (2011)
87. G. Lucazeau, L. Abello, Raman-spectroscopy in solid state physics and materials science - theory, techniques and applications. Analusis **23**, 301 (1995)
88. R. Muccillo, E. N. S. Muccillo, Y. V. França, C. Fredericci, M. O. Prado, E. D. Zanotto, Impedance spectroscopy of a soda-lime glass during sintering. Mater Sci Eng A **352**, 232 (2003)
89. J. Engel, S. R. Bishop, L. Vayssieres, H. L. Tuller, In situ electrical characterization of Anatase TiO_2 quantum dots. Adv Funct Mater **24**, 4952 (2014)
90. P. Knauth, H. Saltsburg, J. Engel, H. L. Tuller, In situ dilatometric and impedance spectroscopy study of core-shell like structures: insights into the exceptional catalytic activity of nanocrystalline Cu-doped CeO_2. J Mater Chem A **3**, 8369 (2015)
91. P. Knauth, J. Engel, S. R. Bishop, H. L. Tuller, Study of compaction and sintering of nanosized oxide powders by in situ electrical measurements and dilatometry: Nano CeO_2-case study. J Electroceram **34**, 82 (2015)
92. R. E. W. Casselton, Blackening in yttria stabilized zirconia due to cathodic processes at solid platinum-electrodes. J Appl Electrochem **4**, 25 (1974)
93. J. Janel, C. Korte, Electrochemical blackening of yttria-stabilized zirconia-morphological instability of the moving reaction front. Solid State Ionics **116**, 181 (1999)
94. S.-W. Kim, S. G. Kim, J.-I. Jung, S.-J. L. Kang, I.-W. Chen, Enhanced grain boundary mobility in Yttria-Stabilized cubic zirconia under an electric current. J Am Ceram Soc **94**, 4231 (2011)
95. S. G. M. Carvalho, E. N. S. Muccillo, R. Muccillo, *Electric field-assisted sintering of zirconia-3 mol% yttria, 38th international*

conference and exposition of advanced ceramics and composites (ICACC'14) (Daytona Beach, FL, USA, 2014)
96. S.G.M. Carvalho, E.N.S. Muccillo, R. Muccillo, Effect of the AC electric field frequency on the microstructure and electrical properties of zirconia-based solid electrolytes (2016) unpublished
97. J. G. Fletcher, A. R. West, J. T. S. Irvine, The AC impedance response of the physical Interface between yttria-stabilized zirconia and $YBa_2Cu_3O_{7-x}$. J Electrochem Soc **142**, 2650 (1995)
98. M. C. Steil, F. Thevenot, M. Kleitz, Densification of Yttria-stabilized zirconia-impedance spectroscopy analysis. J Electrochem Soc **144**, 390 (1997)
99. M. Kleitz, H. Bernard, E. Fernandez, P. Fabry, in Science and Technology of Ceramics, Advances in Ceramics, vol. 9, ed. By A.H. Heuer, L.W. Hobbs The American ceramic society, Inc., Columbus, OH, 1981), p. 310
100. A. Krell, P. Blank, Grain-size dependence of hardness in dense submicrometer alumina. J Am Ceram Soc **78**, 1118 (1995)
101. http://www.tosoh.com/our-products/advanced-materials/zirconia-powders
102. X. Guo, C. Q. Tang, R. Z. Yuan, Grain boundary ionic conduction in zirconia-based solid-electrolyte with alumina addition. J Eur Ceram Soc **15**, 25 (1995)
103. C.-T. Chen, C. E. Danel, S. Kim, On the origin of the blocking effect of grain-boundaries on proton transport in yttrium-doped barium zirconates. J Mater Chem **21**, 5435 (2011)
104. X. Guo, R. Waser, Electrical properties of the grain boundaries of oxygen ion conductors: acceptor-doped zirconia and ceria. Prog Mater Sci **51**, 151 (2006)
105. T. K. Gupta, W. G. Carlson, A grain-boundary defect model for instability/stability of a ZnO varistor. J Mater Sci **20**, 3487 (1985)
106. R. Muccillo, Impedance spectroscopy analysis of zirconia:8 mol% yttria solid electrolytes with graphite pore former. J Mater Res **24**, 1780 (2009)